Polarized Infrared Absorption Spectrum of Matrix-Isolated Methylperoxyl Radicals, CH_3OO $\tilde{X}$ $^2A''$†

Sreela Nandi,‡ Stephen J. Blanksby,‡ Xu Zhang,‡ Mark R. Nimlos,*,‡,§ David C. Dayton,§ and G. Barney Ellison*,‡

Department of Chemistry and Biochemistry, University of Colorado, Boulder, Colorado 80309-0215, and National Renewable Energy Laboratory, 1617 Cole Blvd., Golden, Colorado 80401

Received: July 12, 2001; In Final Form: October 1, 2001

We have used a tandem pair of supersonic nozzles to produce clean samples of CH_3OO radicals in cryogenic matrices. One hyperthermal nozzle decomposes azomethane (CH_3NNCH_3) to generate intense pulses of CH_3 radicals, while the second nozzle alternately fires a burst of O_2/Ar at the 20 K matrix. The CH_3/O_2/20 K argon radical sandwich acts to produce target methylperoxyl radicals: $CH_3 + O_2 \rightarrow CH_3OO$. The absorption spectra of the radicals are monitored with a Fourier transform infrared spectrometer. We report 10 of the 12 fundamental infrared bands of the methylperoxyl radical CH_3OO, $\tilde{X}$ $^2A''$, in an argon matrix at 20 K. The experimental frequencies (cm^{-1}) and polarizations follow: the a′ modes are 3032, 2957, 1448, 1410, 1180, 1109, 902, 492, while the a″ modes are 3024 and 1434. We cannot detect the asymmetric CH_3 rocking mode, ν_{11}, nor the torsion, ν_{12}. The infrared spectra of $CH_3{}^{18}O{}^{18}O$, $^{13}CH_3OO$, and CD_3OO have been measured as well in order to determine the isotopic shifts. The experimental frequencies, $\{\nu\}$, for the methylperoxyl radicals are compared to harmonic frequencies, $\{\omega\}$, resulting from a UB3LYP/6-311G(d,p) electronic structure calculation. Linear dichroism spectra were measured with photooriented radical samples in order to establish the experimental polarizations of most vibrational bands. The methylperoxyl radical matrix frequencies listed above are within ±2% of the gas-phase vibrational frequencies. A final set of vibrational frequencies for the CH_3OO radical are recommended. See also http://ellison.colorado.edu/methylperoxyl.

I. Introduction

The methylperoxyl radical, CH_3OO, is an important intermediate in the oxidation of methane.[1−3] Both in internal combustion engines and in the atmosphere, inorganic radicals "activate" methane by generating the methyl radical which rapidly combines with oxygen. The resulting methylperoxyl radical plays a major role in the oxidation of NO to NO_2. And NO_2 is the immediate precursor to ozone smog and a major driving force in urban air pollution.[4,5]

$$CH_4 + OH \rightarrow CH_3 + H_2O \quad (1a)$$

$$CH_3 + O_2 + M \rightarrow CH_3OO + M \quad (1b)$$

$$CH_3OO + NO \rightarrow [CH_3OONO]^{\ddagger} \rightarrow CH_3O + NO_2 \quad (1c)$$

$$NO_2 + \text{sunlight} \rightarrow NO + O(^3P) \rightarrow O_3\ (\text{"ozone smog"}) \quad (1d)$$

Alkylperoxyl radicals, ROO, are also key intermediates in the heterogeneous oxidation of hydrocarbons. Atmospheric processing of organic aerosols[6] has recently been predicted to be a key step in the nucleation of clouds. Aerosols are μm-sized atmospheric particles that nucleate all clouds and ice particles.[7] In a qualitative manner, an organic aerosol is oxidatively activated in much the same way as gaseous hydrocarbons, only now H atom abstraction takes place from a hydrocarbon film. Recent kinetic studies of OH reacting with organic films coating the walls of a flow tube[8] demonstrate that the hydroxyl radicals are quickly destroyed by collisions with the hydrocarbon film. Equation 2 is a schematic diagram of OH reactive collisions with a film of surfactants coating a μm-sized aerosol. Secondary

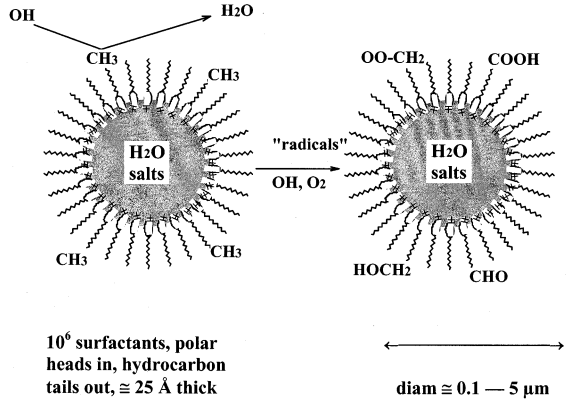

(2)

collisions with O_2 rapidly produce surface-bound alkylperoxyl radicals, $-CH_2OO$. So, in addition to its importance in homogeneous gas-phase chemistry, CH_3OO may well represent an important model system for surface-bound peroxyl radicals on an aerosol, $-CH_2OO$.

In this paper, we report an efficient means to produce and trap the CH_3OO radical in a low-temperature Ar matrix and the matrix-isolated infrared absorption spectrum of this species. In addition to the parent molecule, CH_3OO, we report the

† Part of the special issue "G. Wilse Robinson Festschrift".

* Corresponding authors. E-mail: nimlosm@tcplink.nrel.gov. E-mail: barney@jila.colorado.edu.

‡ University of Colorado.

§ National Renewable Energy Laboratory.

10.1021/jp0126816 CCC: $22.00
Published on Web 12/19/2001

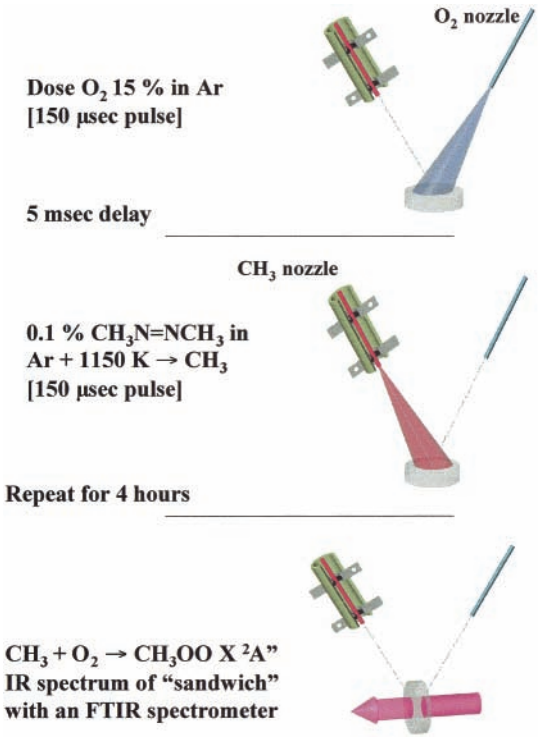

Figure 1. The set of tandem, pulsed nozzles used to produce the CH_3OO radicals; both are fired at a rate of 100 Hz. A Parker General valve is opened for 150 μsec and doses a [15%, 85%] mixture of oxygen and argon onto the 20 K CsI window. Following a 5 ms delay, the hyperthermal nozzle, heated to a wall temperature of 1150 K, is opened for 150 μsec and a 0.1% mixture of azomethane in argon is deposited. The heated nozzle decomposes most of the azomethane to CH_3 radicals and N_2. Each pulse of the hyperthermal nozzle delivers about 3×10^{16} argon atoms pulse^{-1} and approximately 3×10^{13} CH_3 radicals pulse^{-1}. The [O_2/argon], [CH_3NNCH_3/CH_3/N_2/argon] pulse sequence is repeated for roughly 4 h. Then the CsI window is rotated into the FTIR beam for analysis.

infrared spectra of the isotopic-substituted radicals: $CH_3{}^{18}O{}^{18}O$, $^{13}CH_3OO$, and CD_3OO. We have used a polarized Nd:YAG laser to photoorient radicals in the matrix. This enables us to measure the linear dichroism (LD) spectra; consequently we have measured the IR absorption frequencies and polarizations (a′ or a″) for all but two of the vibrational modes of the methylperoxyl radical. The set of experimental methylperoxyl vibrational frequencies, $\{\nu\}$, is compared to UB3LYP/6-311G(d,p) harmonic frequencies, $\{\omega\}$. A final set of vibrational frequencies for the, CH_3OO, $\tilde{X}\ ^2A''$ radical is recommended.

II. Experimental Section

Most methods of alkyl peroxyl radical production involved the initial production of an alkyl radical[5,9] with subsequent three-body reactions with O_2.

$$CH_3 + O_2 + [M] \rightarrow CH_3OO + [M] \qquad (3)$$

We take a similar approach in this work and first establish a methyl radical source then develop a general scheme for production and cryogenic trapping of CH_3OO via reaction 3. Our approach is outlined in Figure 1.

First, the methyl radical production is optimized. Our dosing nozzle for methyl radical production is the hyperthermal nozzle described earlier.[10,11] This is a modified version of the device developed by Chen et al.[12−14] Briefly this consists of a resistively heated 1-mm diameter SiC tube at the output of a Parker General Valve Series 9 pulsed solenoid supersonic valve. This hyperthermal nozzle can be heated to 1700 K to thermally dissociate a radical precursor; the radical's residence time in the hyperthermal nozzle is approximately 100 μs. The two methyl radical precursors used in this work are CH_3I and $CH_3N{=}NCH_3$. The methyl iodide precursor was purchased from Aldrich Chemical Co. while the azomethane precursor was synthesized according to the procedure of Renaud and Leith.[15] Both precursors were used in the production of the CH_3OO parent molecule and frequencies and intensities in the resulting IR spectrum were matched. The $CH_3N{=}NCH_3$ precursor was used along with $^{18}O_2$ from Isotech to produce the $CH_3{}^{18}O{}^{18}O$ isotopomer. Respectively, $^{13}CH_3I$, CD_3NNCD_3, and CD_3I were used in the production of the $^{13}CH_3OO$ and CD_3OO isotopomers. The preparation of $CD_3N{=}NCD_3$, d_6-azobismethane, is not commonly available so we have found a convenient route.[16−18] This is described in Appendix A of this paper.

To optimize the (CH_3I, $CH_3N{=}NCH_3$) pyrolysis conditions, the hyperthermal nozzle was interfaced with a photoionization mass spectrometer.[11,19] The skimmed output of the nozzle was crossed with 118.2 nm (10.487 eV) light from the 9th harmonic of a YAG laser. Entrained molecules with an ionization potential less than 10.5 eV are ionized and analyzed by a reflectron time-of-flight spectrometer. Mass spectra for each precursor were measured as a function of pyrolysis temperature. At 1200 K, only CH_3^+ (m/z 15) was detected. The nozzle is thus operated between 1200 and 1300 K during dosing experiments.

The dosing valve for the O_2 was a second Parker General Valve Series 9 pulsed solenoid supersonic valve with a 1/16 in. stainless tube at the output aperture. Both this valve and the hyperthermal nozzle were fitted with 100 μm circular output orifices. The hyperthermal nozzle was mounted to the vacuum shroud of an ADP cryostat inside a water-cooled minichamber. The second valve was attached to this vacuum shroud by attaching the stainless steel tube via an O-ring sealed compression fitting on the side of the shroud. These valves were positioned at a 45° angle with respect to one another and are approximately 2.5 cm away from the cryogenic CsI sample. The hyperthermal valve has approximately a 150 μs pulse width and a stagnation pressure of 1.2 atm, with a 1.2 L stagnation reservoir. The gas mixture for the low temperature dosing valve was made at 1.2 atm stagnation pressure in a 2 L gas reservoir. A line regulator between the stagnation reservoir and the low temperature valve was held at approximately 0.5 atm. Both valves have an opening pulse width of approximately 150 μs. The pressure drop in each stagnation reservoir was measured using a capacitance manometer to determine the gas throughput. One beam was dosed at a time on a 20 K window so that one layer of argon and entrained reactant is deposited at a time (Figure 1). We create alternating monolayers of reactants, creating a multilayer sandwich matrix. The repetition rate in this experiment was 100 Hz, the maximum repetition rate at which the solenoid valves can operate.

Once the radicals are trapped in the matrix, the temperature was lowered to 12 K and the infrared spectrum of the sample was measured. We use a Nicolet Magna 550 Fourier transform infrared spectrometer with a mercury/cadmium/telluride (MCT-B) detector to measure the spectrum. The APD cryostat is equipped with a pair of CsI side windows through which the interrogating IR beam from the instrument passes. These windows and the CsI sample window attenuate the IR beam by a factor of 3. When the CsI sample window is dosed with pure argon the signal level is attenuated by a factor of roughly 1.5. When the sample window is dosed with the sandwich matrices containing O_2, the signal levels are attenuated by a factor of 5

to 10. After 3 to 5 h of dosing, the most intense IR modes of CH_3OO have a signal level between 0.5 and 1 o.d. for a mixing ratio of 2 parts $CH_3N{=}NCH_3$ to 1000 parts Ar gas. Increased dosing times result in both higher signal levels and lower matrix transparency; thus signal-to-noise ratio actually decreases with longer dosing times. Wire grid polarizers from Molectron (285 to 4000 cm^{-1}) are used to create polarized IR light for the linear dichroism experiments. This polarizer attenuates the signal by an additional factor of 2. The 4th harmonic of a Continuum Nd:YAG laser (266 nm) is used as our UV light source for depleting the trapped methylperoxyl radical. In the polarization experiment, the distribution of methylperoxyl radical is preferentially photooriented by destroying 75 to 90% of the molecules in the matrix. The signal levels are thus attenuated by an additional factor of 10. The linear dichroism signal is a difference signal of measurement of the matrix with horizontally and vertically polarized light. This difference signal is a function of the degree of orientation of the molecules. The degree of orientation is in turn a function of the quantum yield of the photolysis and anisotropy of the dissociative electronic transition. The linear dichroism signal level in this experiment is approximately 200 times lower than the signal level of the dosed matrix before irradiation. The signal-to-noise ratio in linear dichroism experiments is approximately 20 for the three most intense peaks in the IR spectrum of methylperoxyl radical and approximately 1 or 2 for the least intense feature for methylperoxyl radical. The signal levels for methylperoxyl radical generated using methyl iodide precursor were roughly 20 lower than those using the azomethane precursor.

III. Results and Discussion

A. Electronic Structure of the Methylperoxyl Radical and Photoorientation. The electronic structure of the methylperoxyl radical is similar to that of the HO_2 radical.[20] The CH_3OO ground state is $\tilde{X}\ ^2A''$ and there is a low-lying $\tilde{A}\ ^2A'$ excited state in the near-IR. The term value for the $\tilde{A}\ ^2A' \leftarrow \tilde{X}\ ^2A''$ transition was measured[21] in 1976; recent cavity ring down spectroscopy[22] reports $T_0(\tilde{A}\ ^2A' \leftarrow \tilde{X}\ ^2A'') = 7372.6 \pm 0.5$ cm^{-1}. A second, dissociative excited state of CH_3OO ($\tilde{B}\ ^2A''$) is observed[5] near 225−260 nm in the UV spectrum. These states of the CH_3OO radical can be represented in a convenient manner with GVB diagrams.[20,23,24]

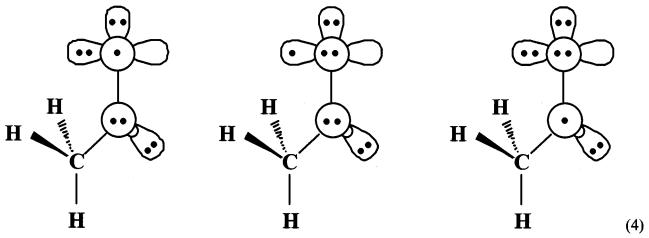

Recent photodetachment studies[25] of the $CH_3O_2^-$ anion clearly detect the two lowest states of methylperoxyl, CH_3OO ($\tilde{X}\ ^2A''$) and CH_3OO ($\tilde{A}\ ^2A'$), and measure the adiabatic electron affinity of the ground state to be $EA[CH_3OO(\tilde{X}\ ^2A'')] = 1.161 \pm 0.005$ eV. These studies also report the vibrational frequencies corresponding to fundamentals of two ground-state modes, $\nu_6[CH_3OO(\tilde{X}\ ^2A'')] = 1124 \pm 5$ cm^{-1} and $\nu_8[CH_3OO(\tilde{X}\ ^2A'')] = 482 \pm 9$ cm^{-1}. A combination[26] of the electron affinity, gas-phase acidity measurements, and high level ab initio electronic structure calculations[27] gives the heat of formation of the methylperoxyl radical as $\Delta_f H_{298}(CH_3OO) = 4.8 \pm 1.2$ kcal mol^{-1}, and thus a heat of reaction of $\Delta_{rxn}H_{298}[CH_3 + O_2 \rightarrow CH_3OO] = -30.1 \pm 1.2$ kcal mol^{-1} for the preparation of CH_3OO radicals as undertaken here (eq 3).

TABLE 1: Local Symmetry Modes $\{S\}_{i=1,8}$ of the CH_3-X Group

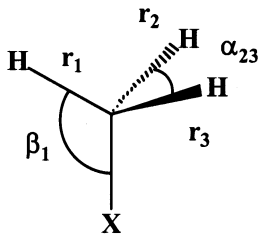

		$\nu[CH_3F]$/ cm^{-1}	local CH_3 mode
S_1	sym stretch	2930	$(\Delta r_1 + \Delta r_2 + \Delta r_3)/\sqrt{3}$
S_2	umbrella	1464	$(\Delta\alpha_{12} + \Delta\alpha_{13} + \Delta\alpha_{23} - \Delta\beta_1 - \Delta\beta_2 - \Delta\beta_3)/\sqrt{6}$
S_3	deg. stretch	3006	$(2\Delta r_1 - \Delta r_2 - \Delta r_3)/\sqrt{6}$ $(\Delta r_2 - \Delta r_3)/\sqrt{2}$
S_4	deg. deformation	1467	$(2\Delta\alpha_{23} - \Delta\alpha_{31} - \Delta\alpha_{12})/\sqrt{6}$ $(\Delta\alpha_{31} - \Delta\alpha_{12})/\sqrt{2}$
S_5	deg. rock	1182	$(2\Delta\beta_1 - \Delta\beta_2 - \Delta\beta_3)/\sqrt{6}$ $(\Delta\beta_2 - \Delta\beta_3)/\sqrt{2}$

As eq 4 indicates, the methylperoxyl radical is a molecule with a plane of symmetry. This C_s species possesses 12 vibrational modes and all are infrared active: $\Gamma_{vib}(CH_3OO) = 8a' \oplus 4a''$. We anticipate there are three high-frequency C−H vibrations ($2a' \oplus 1a''$ modes about 3000 cm^{-1}) and one low-frequency CH_3-OO torsional vibration (a'' mode less than 200 cm^{-1}). This leaves eight modes ($6a' \oplus 2a''$) in the frequency range 500−1500 cm^{-1}.

A chemist might anticipate that the vibrational modes of the methylperoxyl radical are roughly a set of methyl modes that are perturbed by O_2: CH_3-OO. Consequently, it is useful to decompose the 8 "CH_3-related" modes in CH_3-X to C_{3v} symmetry modes $\{S\}_8$ (we ignore the C−X stretch mode). Table 1 lists these modes[28,29] as the symmetric stretch (S_1), the umbrella mode (S_2), the degenerate stretch (S_3), the degenerate deformation (S_4), and the degenerate rock (S_5). To get a feel for the magnitude of these frequencies, we list the experimental values[30] for the methyl group in CH_3F. We have carried a set of DFT electronic structure calculations[31] and extracted the set of harmonic vibrational frequencies $\{\omega\}$ for the CH_3OO $\tilde{X}\ ^2A''$ radical. These are UB3LYP/6-311G(d,p) calculations and the (unscaled) results are collected in Table 2. One can view[32] the animated harmonic modes and assign each of them to a local mode. The local modes $\{R\}$ are the CH_3-X symmetry modes $\{S\}$ from Table 1. As the symmetry of the CH_3 group is broken from C_{3v} to C_s, each of the e modes in Table 1 splits into an [$a' \oplus a''$] pair. The symmetric component of the CH_3 degenerate rock, R_{5a}, strongly mixes with the O−O stretch, R_{OO}, and the (±pair) becomes (ω_5, ω_6) of the CH_3OO radical.

In a set of remarkable pioneering studies, Snelson's laboratory has reported the partial matrix infrared spectra of several alkylperoxyl radicals.[33−37] The ROO radicals were prepared by [R + O_2] recombination reactions in a cryogenic matrix. The alkyl radicals [CH_3, CH_3CH_2, $(CH_3)_2CH$, and $C(CH_3)_3$] were prepared in an effusive source by pyrolysis of an appropriate precursor. In the case of methylperoxyl radical, this gas-phase CH_3 radical production and matrix deposition occurred over a period of 1 to 3 days. Because they used an effusive source, which presumably had a longer residence time in the pyrolytic

TABLE 2: UB3LYP/6−311 G(p,d) Harmonic Frequencies (ω/cm^{-1}) and Infrared Intensities (A/km mol^{-1}) for the $\tilde{X}$ ^{2}A″ Methylperoxyl Radical (all values unscaled)[a]

			CH_3OO		$CH_3{}^{18}O^{18}O$		$^{13}CH_3OO$		CD_3OO	
	mode	local mode	ω/cm^{-1}	A/km mol^{-1}	ω/cm^{-1}	A/km mol^{-1}	ω/cm^{-1}	A/km mol^{-1}	ω/cm^{-1}	A/km mol^{-1}
a′	ω_1	R_{3a}	3155	10.7	3155	10.7	3143	10.5	2344	7.8
	ω_2	R_1	3048	13.8	3048	13.8	3045	13.5	2179	9.3
	ω_3	R_{4a}	1484	9.9	1483	9.6	1482	10.2	1201	9.0
	ω_4	R_2	1445	0.8	1443	0.9	1438	0.7	1094	6.1
	ω_5	$R_{5a} + R_{OO}$	1217	9.3	1194	5.5	1211	9.4	1068	1.0
	ω_6	$R_{5a} - R_{OO}$	1155	2.0	1104	4.8	1150	1.5	995	4.0
	ω_7	CH_3-O_2 stretch	914	12.9	892	12.9	898	12.0	832	9.6
	ω_8	CH_3-O-O bend	494	6.4	477	5.9	490	6.5	448	4.7
a″	ω_9	R_{3b}	3138	15.8	3138	15.8	3126	15.4	2331	10.7
	ω_{10}	R_{4b}	1470	10.4	1470	10.4	1468	10.6	1061	4.0
	ω_{11}	R_{5b}	1128	0.6	1126	0.6	1121	0.5	867	1.8
	ω_{12}	CH_3-O-O torsion	138	0.1	136	0.1	138	0.1	109	0.1

[a] To view the animated vibrational modes, see http://ellison.colorado.edu/methylperoxyl.

TABLE 3: Earlier Matrix Assignments (ν/cm^{-1}) of Ase et al. for Methylperoxyl Radical[33,34,44]

mode		local mode	CH_3OO	$CH_3{}^{18}O^{18}O$	$^{13}CH_3OO$	CD_3OO
3		CH_3 deformation	1453	1450	1451	
4		CH_3 deformation	1440	1438	1438	1048
5		CH_3 rock	1183	1169	1175	
6		O−O stretch	902	880	888	821
7		C−O stretch	1112	1056	1110	1146
8		C−O−O bend	492	476	487	445
9	a″	CH_3 asym stretch	2968	2968	2960	2176
10		CH_3 deformation	1414	1412	1407	1078
11		CH_3 rock		1115		860

region, Ase et al. had to contend with significant production of other contaminating hydrocarbons and oxygenated species as well as dimerization of methylperoxyl radical. While Ase et al. were able to study 10 isotopic variants of methylperoxyl radical, only frequencies for the set that compare to our work[33,34] [CH_3OO, $CH_3{}^{18}O^{18}O$, $^{13}CH_3OO$, and CD_3OO] are listed in Table 3.

The methylperoxyl radical has C_s symmetry and there is a broad electronic transition in CH_3OO from 200 to 300 nm centered at 250 nm to the $\tilde{B}$ ^{2}A″ state.[5] Consequently, the transition matrix element [$\langle\tilde{B}\ ^2A''|\mu|\tilde{X}\ ^2A''\rangle$] yields the symmetry of the transition moment to be A′. We excite our isotropic distribution of CH_3OO trapped in the matrix using polarized 266 nm light and deplete our target radical until 75 to 90% of the identified CH_3OO IR fundamental lines are bleached. This depleting laser light is horizontally polarized with respect to the laboratory frame, the *Z* direction. Any molecule that has a significant projection of its transition dipole moment, μ, parallel to the depleting laser light will be preferentially depleted.[38] The remaining CH_3OO molecules will be preferentially oriented with their transition dipole moments perpendicular to the depleting laser light. We then measure the IR spectrum of the remaining distribution of the trapped radicals using IR light both horizontally and vertically polarized with respect to the laboratory frame, the *Z* and *Y* directions. The absorption intensity for the a′ modes (parallel to transition dipole moment) will be greater using IR light polarized in the *Y* direction (vertically polarized IR light) and be less using IR light polarized in the *Z* direction (horizontally polarized IR light). That is, $I_Y - I_Z > 0$ (exhibit positive linear dichroism or LD) for modes of a′. Correspondingly, absorption intensities for a″ modes will be lower using vertically oriented (*Y* direction) IR light for measurement; that is, $I_Y - I_Z < 0$ (exhibit negative linear dichroism or LD) for modes of a″ symmetry.

B. Assignments of the Methylperoxyl Radical IR Spectra. Figure 2 is an overview of the entire infrared absorption spectrum of the methylperoxyl radical, CH_3OO, $\tilde{X}$ ^{2}A″. The experimental IR spectrum is the black trace, and each of the assigned methylperoxyl radical fundamentals is marked by a bullet (•). Colored red and offset above the IR absorption spectrum are the DFT calculated harmonic predictions {ω} [UB3LYP/6−311-G(d, p)] from Table 2. The calculated harmonic frequencies and intensities in Table 2, and in all figures, are unscaled. The low-frequency CH_3-O-O torsional a″ mode, ω_{12}, is not shown because it is predicted to appear at 138 cm^{-1}, far below the range of our MCT detector. As mentioned earlier, the irreducible representations of the methylperoxyl radical vibrations are: $\Gamma_{vib}(CH_3OO) = 8a' \oplus 4a''$. Consequently, there are 11 red peaks marked on the spectrum in Figure 2 (12 modes of CH_3OO, less the torsional a″ mode, ω_{12}).

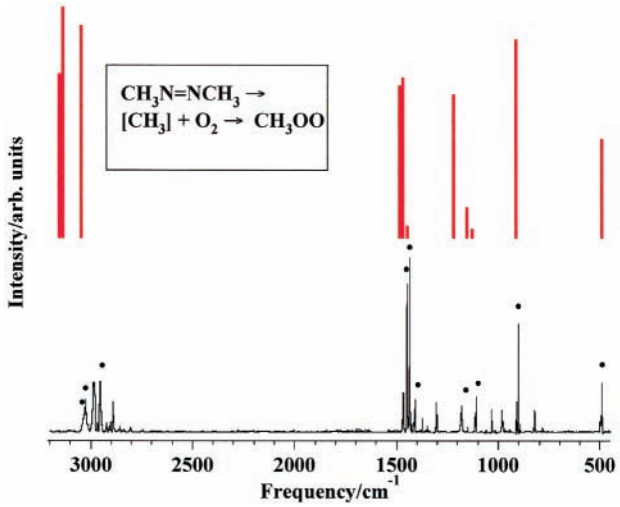

Figure 2. An overview of the infrared absorption spectrum of matrix isolated methylperoxyl radical. Methyl radicals are produced by the thermal dissociation of $CH_3N{=}NCH_3$ in a hyperthermal nozzle at 1200 K; they combine with O_2 in the matrix to generate CH_3OO radicals. The solid, black trace is the experimental IR spectrum and the fundamental infrared modes, {ν}, are marked by bullets (•). The DFT calculated [UB3LYP/6−311-G(d,p)] harmonic frequencies, {ω}, are plotted as red sticks.

The 266 nm depleted IR spectrum of CH_3OO is shown on the top of Figure 3. (in black). Since the $\tilde{B}$ ^{2}A″ state of CH_3OO is dissociative, we expect the vibrational fundamentals of the methylperoxyl radical to be depleted. The IR bands that grow in belong to the 266 nm photoproducts of CH_3OO. Several are identified at the top of Figure 3: HCHO, HO_2, O_3, and CH_3. The red trace at the bottom of Figure 3 is the 266 nm LD spectrum of CH_3OO. The IR absorption bands that are a′ are positive while the a″ modes are negative. Figure 3 shows the

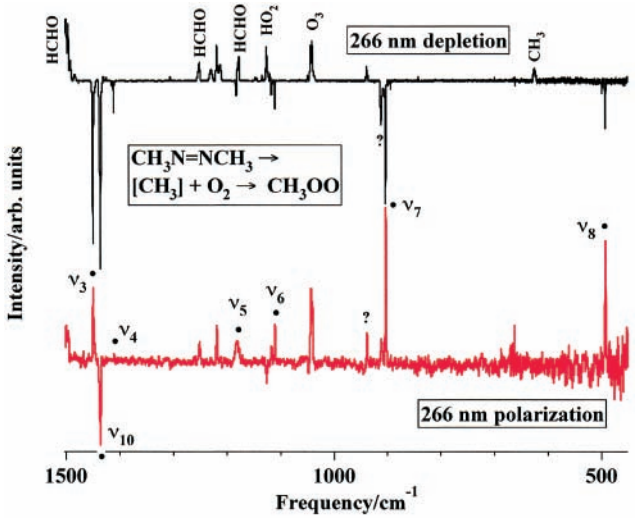

Figure 3. There are two separate spectra here. At the top, in black, is an infrared spectrum showing the depletion of matrix isolated CH_3OO radicals "fingerprint region" upon bombardment by 266 nm laser light. On the bottom, in red, is a linear dichroism spectrum of the CH_3OO radical following matrix depletion by polarized 266 nm light. IR bands of CH_3OO that are a″ polarized will have a negative dichroism while IR features with a′ polarization will have a positive dichroism. The infrared fundamentals of the CH_3OO radical are marked by bullets (•).

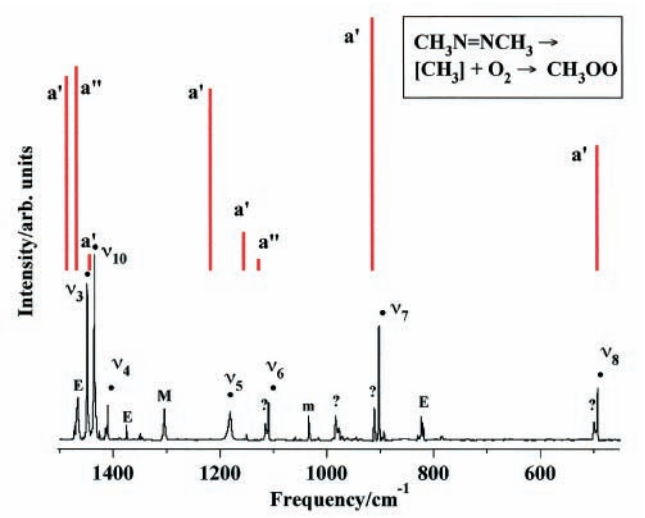

Figure 4. A comparison of the calculated and experimental fingerprint regions of the methylperoxyl radical. The DFT harmonic frequencies $\{\omega\}$ in red reproduce the experimental fundamentals $\{\nu\}$ marked by bullets (•). Interfering species are marked as **E** (CH_3CH_3), **M** (CH_4), and **m** (CH_3OH). The ordering of the harmonic modes is a nearly perfect match to the experimental modes $\{\nu\}$: ω_3(a′), ω_{10}(a″), ω_4(a′), ω_5(a′), ω_6(a′), ω_{11}(a″), ω_7(a′), and ω_8(a′). As mentioned in the text, we do not observe ν_{11} so ω_{11}(a″) has no match.

only a″ mode, ν_{10}, at a frequency 1434 cm^{-1}. This mode is the most intense band in the vibrational spectrum of the methylperoxyl radical and will be assigned as an antisymmetric CH_3 deformation derived from S_4 in Table 1. The remaining a′ IR bands at the bottom of Figure 3 [ν_3, ν_4, ν_5, ν_6, ν_7, and ν_8] match up exactly with a depleted band in the photodissociation spectrum at the top of Figure 3 (black trace).

Figure 4 is a detailed comparison of the DFT harmonic frequencies (top bands in red) with the experimental vibrational features (marked by •). The ordering of harmonic bands $\{\omega\}$ exactly matches the assigned IR bands. As an example, consider that the closely spaced features $\{\omega_3$(a′), ω_{10}(a″), and ω_4(a′)$\}$ are ordered precisely as $\{\nu_3$(a′), ν_{10}(a″), and ν_4(a′)$\}$. The weak

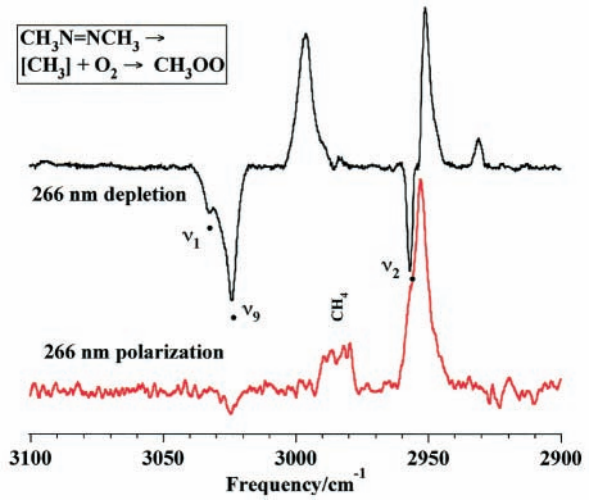

Figure 5. At the top, in black, is an infrared spectrum showing the depletion of matrix isolated CH_3OO radicals, "CH region", upon bombardment by 266 nm laser light. On the bottom, in red, is a linear dichroism spectrum of the CH_3OO radical following matrix depletion by polarized 266 nm light. IR bands of CH_3OO that are a″ polarized will have a negative dichroism while IR features with a′ polarization will have a positive dichroism. The three infrared fundamentals of the CH_3OO radical are marked by bullets (•).

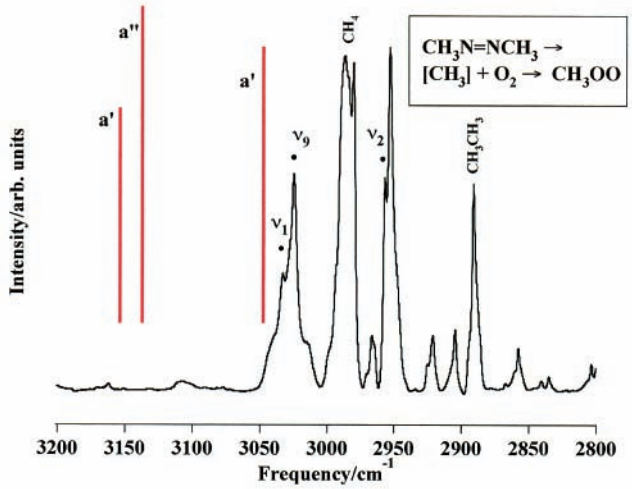

Figure 6. A comparison of the CH region of the methylperoxyl radical. The DFT harmonic frequencies $\{\omega\}$ in red reproduce the experimental fundamentals $\{\nu\}$ marked by bullets (•). There are intense interferences from CH_4 and CH_3CH_3.

a″ vibrational mode, ν_{11}, could not be detected; the harmonic mode, ω_{11} at 1128 cm^{-1}, is predicted to be weak (0.6 km mol^{-1} in Table 2).

Figure 5 is a trace of the depletion spectrum of the CH region (top of figure in black) and the 266 LD dichroism spectrum (bottom trace in red). The depletion spectrum shows three bands as expected. The (red) LD spectrum below is disappointing in that it yields only two CH_3OO features. One of these, ν_9, is clearly an a″ band while the a′ shoulder at 2954 cm^{-1} matches the ν_2 depletion. Since there are three hydrogen atoms in CH_3OO, there must be three CH stretches; by group theory there will be two a′ CH bands and one a″ CH feature. The weak feature at 3024 cm^{-1} is a″ polarized; consequently all three bands in the depletion spectrum can be assigned as ν_1, ν_9, and ν_2. Figure 6 is a comparison of the harmonic CH modes (three red bands) with the experimental features (•). Our final assignments for the CH_3OO vibrational fundamentals are summarized in Table 4.

TABLE 4: Experimental Vibrational Frequencies (ν/cm^{-1}) and Relative Infrared Intensities (A/km mol^{-1} as % of the base peak) for Matrix-Isolated $\tilde{X}\ ^2A''$ Methylperoxyl Radical[a]

		CH_3OO			$CH_3{}^{18}O{}^{18}O$			$^{13}CH_3OO$			CD_3OO		
		ν/cm^{-1}	A(%)	pol'n	ν/cm^{-1}	A(%)	pol'n	ν/cm^{-1}	A(%)	pol'n	ν/cm^{-1}	A(%)	pol'n
a′	ν_1	3032			3033			3021			2280	42	
	ν_2	2954		+	2953		+	2948	31		2172	76	
	ν_3	1448	71	+	1448	85	+	1447	59	+	1144	119	+
	ν_4	1410	8	+	1408	10		1404	19		1076	124	+
	ν_5	1180	37	+	1165	39	+	1173	37		1050	24	
	ν_6	1109	25	+	1055	51	+	1104	23		941	31	
	ν_7	902	78	+	880	109	+	887	64	+	822	190	+
	ν_8	492	30	+	477	35	+	487	32	+	446	30	+
a″	ν_9	3024		−	3022		−	3014			2273	163	
	ν_{10}	1434	100	−	1434	100	−	1432	100	−	1046	100	−
	ν_{11}	na			na			na			860	32	−
	ν_{12}	na			na			na			na		

[a] The symbol na means the mode was not observed and hence not available. See Figures 2−16 for details.

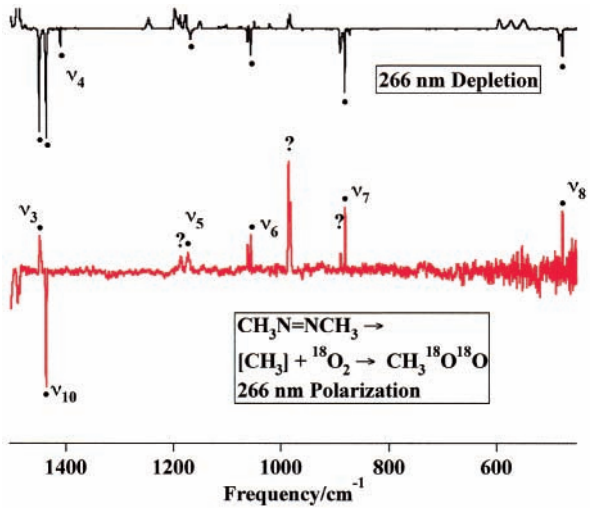

Figure 7. At the top, in black, is an infrared spectrum showing the depletion of matrix isolated $CH_3{}^{18}OO$ radicals, "fingerprint region", upon bombardment by 266 nm laser light. On the bottom, in red, is a linear dichroism spectrum of the $CH_3{}^{18}OO$ radical following matrix depletion by polarized 266 nm light. IR bands of CH_3OO that are a″ polarized will have a negative dichroism while IR features with a′ polarization will have a positive dichroism. The infrared fundamentals of the $CH_3{}^{18}OO$ radical are marked by bullets (•).

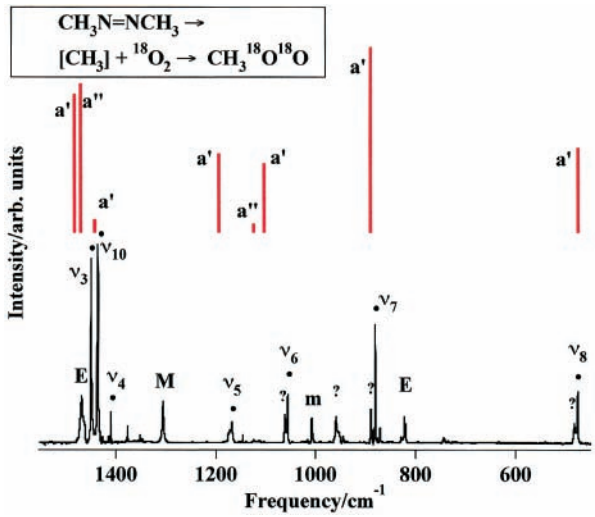

Figure 8. A comparison of the calculated and experimental fingerprint region of the $CH_3{}^{18}OO$ methylperoxyl radical. The DFT harmonic frequencies $\{\omega\}$ in red reproduce the experimental fundamentals $\{\nu\}$ marked by bullets (•). Interfering species are marked as **E** (CH_3CH_3), **M** (CH_4), and **m** (CH_3OH).

In addition to the parent CH_3OO radical, we have also prepared and examined several isotopomers of the methylperoxyl radical: $CH_3{}^{18}O{}^{18}O$, $^{13}CH_3OO$, and CD_3OO. These spectra are collected and discussed in Appendix B.

IV. Conclusions

One useful test of the assigned harmonic frequencies $\{\omega\}$ of Tables 1 and 2 is to see if they reproduce the set of small frequency shifts $\{\Delta\nu\}$ as the atoms in the CH_3OO radical are isotopically substituted. The set of experimental frequencies for the methylperoxyl radical (Table 4) are reasonably reproduced by the UB3LYP/6−311-G(d,p) harmonic frequencies in Table 2 as shown by Figures 2, 4, 6, 8, 10, 12, 13, 15, and 16. A direct comparison of the experimental frequency shifts of the CH_3OO, $CH_3{}^{18}O{}^{18}O$, and $^{13}CH_3OO$ isotopomers, $\{\Delta\nu\}$, with the corresponding harmonic shifts, $\{\Delta\omega\}$, confirms our assignments. For example, Table 4 indicates that the intense a′ CH_3-O_2 stretching mode, ν_7, shifts by 22 cm^{-1} in the $CH_3{}^{18}O{}^{18}O$ isotopomer [902−880 cm^{-1}] and by 15 cm^{-1} in the $^{13}CH_3OO$ isotopomer [902−887 cm^{-1}]; Table 2 shows that the predicted harmonic shifts in ω_7 are 22 and 16 cm^{-1}, respectively. Table 5 has such a comparison for all of the infrared fundamentals, and the results are generally satisfactory. The *absolute* harmonic frequencies are off by roughly 2%−4%, which is consistent with previous B3LYP results on closed shell molecules.[39,40] However, the UB3LYP/6−311-G(d,p) infrared intensities, {A}, for the harmonic modes do not correlate very well with the observed intensities. This may be the fault of the small basis set that we have used to compute $\{\omega\}$. Table 5 indicates that *all* the relative isotopic shifts are faithfully reproduced; we have not included the CD_3OO isotopomer here because of extensive mode mixing.

Before we reach a final conclusion for the gas-phase vibrational frequencies of methylperoxyl, we attempt to estimate the magnitude of the gas-to-matrix frequency shifts. The matrix shifts for a large number of diatomic and small polyatomic free radicals and ions trapped in Ne and Ar matrices has been reviewed.[41,42] It was concluded that for polyatomic free radicals in Ar matrices, the frequency shift is generally less than 1% and usually to the red. We know of no rotationally resolved frequencies available for CH_3OO. The only methylperoxyl frequencies that we are aware of are those observed in the negative ion photoelectron spectrum.[25] Photodetachment of $CH_3O_2^-$ yields the gas-phase values for $\nu_6(CH_3OO\ \tilde{X}\ ^2A'') = 1124 \pm 5$ cm^{-1} and $\nu_8(CH_3OO\ \tilde{X}\ ^2A'') = 482 \pm 9$ cm^{-1}. The methylperoxyl radical matrix IR values from Table 4 are $\nu_6 = 1109$ cm^{-1} and $\nu_8 = 492$ cm^{-1}, which give us an idea of the matrix-to-gas frequency shifts: $\Delta\nu_6 = 15 \pm 5$ cm^{-1} and $\Delta\nu_8$

TABLE 5: Isotopic Shifts (cm^{-1}) of Methylperoxyl Radicals (Tables 2, 4)

			oxygen isotope shift		carbon isotope shift	
	mode	local mode	$\Delta\nu(^{16}O-^{18}O)$	$\Delta\omega(^{16}O-^{18}O)$	$\Delta\nu(^{12}C-^{13}C)$	$\Delta\omega(^{12}C-^{13}C)$
a′	1	R_{3a}	−1	0	11	12
	2	R_1	1	0	6	3
	3	R_{4a}	0	1	1	2
	4	R_2	2	2	6	7
	5	$R_{5a} + R_{OO}$	15	23	7	6
	6	$R_{5a} - R_{OO}$	54	52	5	5
	7	CH_3-O_2 stretch	22	22	15	16
	8	CH_3-O-O bend	15	17	5	4
a″	9	R_{3b}	2	0	10	12
	10	R_{4b}	0	1	2	2
	11	R_{5b}		2		7
	12	CH_3-O-O torsion		2		0

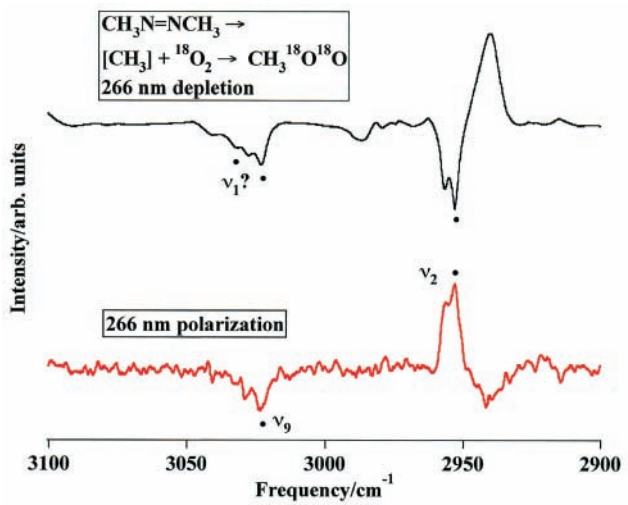

Figure 9. At the top, in black, is an infrared spectrum showing the depletion of matrix isolated $CH_3{}^{18}OO$ radicals, "CH region", upon bombardment by 266 nm laser light. On the bottom, in red, is a linear dichroism spectrum of the $CH_3{}^{18}OO$ radical following matrix depletion by polarized 266 nm light. It is evident that the exact location of both of the a′ modes, ν_1 and ν_2, is not easy.

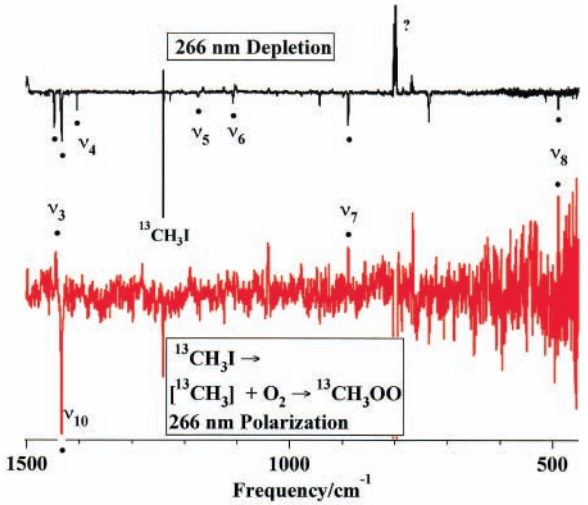

Figure 11. At the top, in black, is an infrared spectrum showing the depletion of the "fingerprint region" of the matrix isolated $^{13}CH_3OO$ radicals upon bombardment by 266 nm laser light. On the bottom, in red, is a linear dichroism spectrum of the $^{13}CH_3OO$ radical following matrix depletion by polarized 266 nm light. The infrared fundamentals of the $^{13}CH_3OO$ radical are marked by bullets (•).

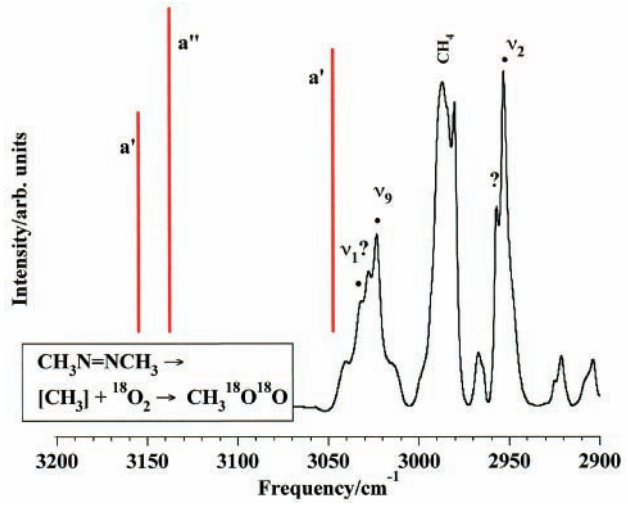

Figure 10. A comparison of the CH region of the $CH_3{}^{18}OO$ methylperoxyl radical. The DFT harmonic frequencies $\{\omega\}$ in red reproduce the experimental fundamentals $\{\nu\}$ marked by bullets (•). There are intense interferences from CH_4.

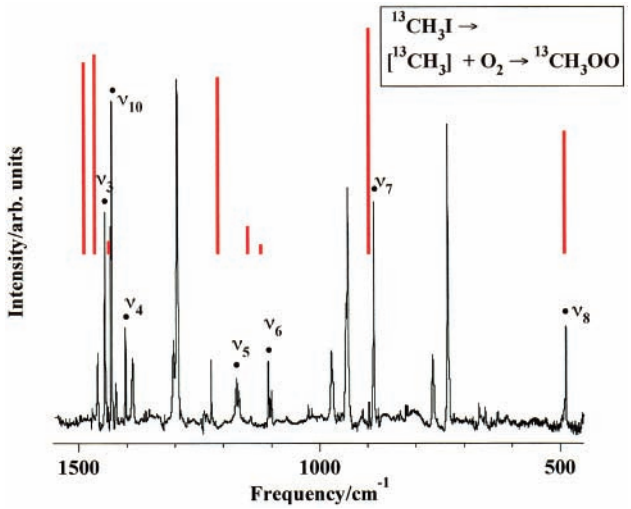

Figure 12. A comparison of the calculated and experimental fingerprint region of the $^{13}CH_3OO$ methylperoxyl radical. The DFT harmonic frequencies $\{\omega\}$ in red reproduce the experimental fundamentals $\{\nu\}$ marked by bullets (•).

$= 10 \pm 9\ cm^{-1}$. Consequently we believe that all of the matrix frequencies for CH_3OO $\tilde{X}\ ^2A''$ in Table 4 are within ≅2% of the true, gas-phase frequencies.

A detailed comparison of our vibrational frequencies for CH_3OO $\tilde{X}\ ^2A''$ (Table 4) with those of Ase et al. (Table 3) reveals general agreement (within 20 or 30 cm^{-1}) for most of the modes except for ν_6 and ν_7. Our data and the negative ion photodeteachment results[25] clearly demonstrate that this earlier study confused the assignment of the (ν_6, ν_7) pair of a′ modes.

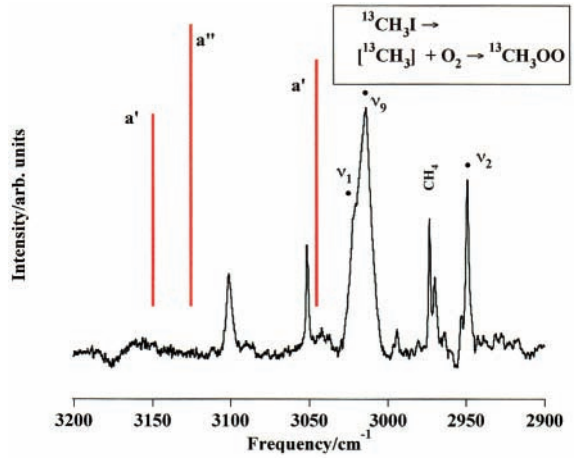

Figure 13. A comparison of the CH region of the $^{13}CH_3OO$ methylperoxyl radical. The DFT harmonic frequencies $\{\omega\}$ in red reproduce the experimental fundamentals $\{\nu\}$ marked by bullets (•). There are intense interferences from CH_4.

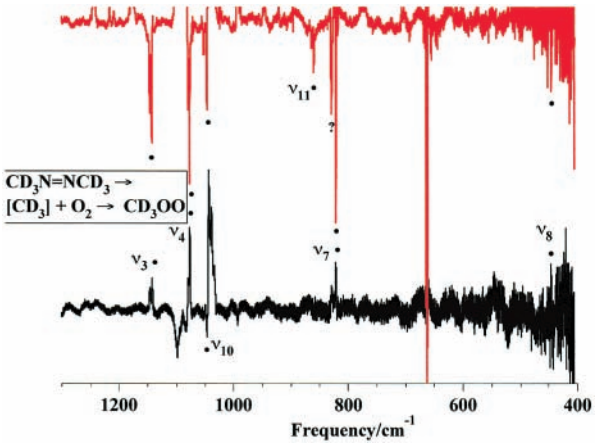

Figure 14. At the top, in red, is an infrared spectrum showing the depletion of the "fingerprint region" of the matrix isolated CD_3OO radical upon bombardment by 266 nm laser light. On the bottom, in black, is a linear dichroism spectrum of the CD_3OO radical following matrix depletion by polarized 266 nm light. The infrared fundamentals of the CD_3OO radical are marked by bullets (•).

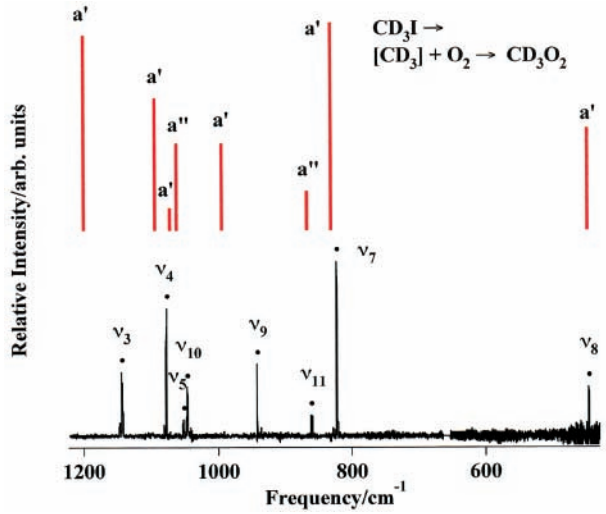

Figure 15. A comparison of the calculated and experimental fingerprint region of the CD_3OO methylperoxyl radical. The DFT harmonic frequencies $\{\omega\}$ in red reproduce the experimental fundamentals $\{\nu\}$ marked by bullets (•).

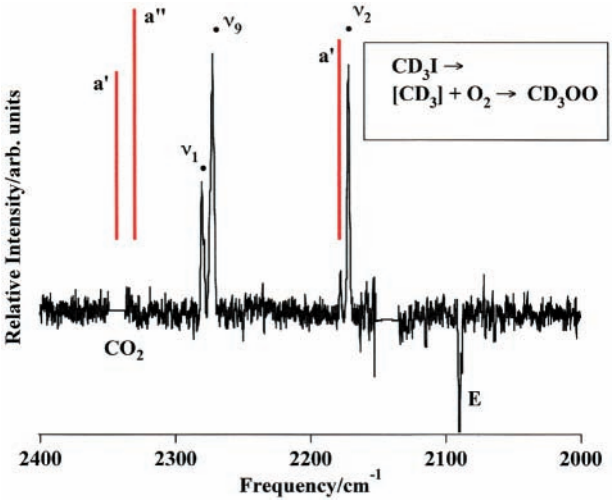

Figure 16. A comparison of the CH region of the CD_3OO methylperoxyl radical. The DFT harmonic frequencies $\{\omega\}$ in red reproduce the experimental fundamentals $\{\nu\}$ marked by bullets (•).

TABLE 6: Recommended Vibrational Frequencies (ν/cm^{-1}) for the Methylperoxyl Radical, $\tilde{X}\ ^2A''$ CH_3OO[a]

	mode	local mode description	ν/cm^{-1}	ref
a′	1	R_{3a}	3032	this work
	2	R_1	2954	this work
	3	R_{4a}	1448	this work
	4	R_2	1410	this work
	5	$R_{5a} + R_{OO}$	1180	this work
	6	$R_{5a} - R_{OO}$	1124 ± 5	25
	7	$CH_3{-}O_2$ stretch	902	this work
	8	$CH_3{-}O{-}O$ bend	482 ± 9	25
a″	9	R_{3b}	3024	this work
	10	R_{4b}	1434	this work
	11	R_{5b}	na	
	12	$CH_3{-}O{-}O$ torsion	na	

[a] The symbol na means the mode was not observed and hence not available.

In addition we have been able to detect all of the CH stretching frequencies and polarizations for the CH_3OO radical.

Finally we recommend a set of vibrational frequencies for the CH_3OO radical in Table 6. The prominent methylperoxyl skeletal bending modes, ν_6 and ν_8, have been observed[25] in the negative ion photodetachment of the peroxide anion: $CH_3O_2^- \rightarrow CH_3OO + e^-$. All the rest of the frequencies in Table 6 are from this matrix infrared study. Our polarization spectroscopy has provided new information that makes many of the fundamental assignments of the CH_3OO radical more definite. The pulsed nozzle techniques of this paper permit us to produce the target methylperoxyl radicals. We observe very narrow IR absorption lines for CH_3OO, and these can be measured with high accuracy; consequently, apart from the unknown matrix shifts, the fundamentals are determined to very high accuracy.

Acknowledgment. This work was supported by grants from the Chemical Physics Program, United States Department of Energy (DE-FG02-87ER13695). G.B.E. also thanks the NSF (CHE-9813659) for support of our surface spectroscopy of organic radicals. The work at NREL was supported by the United States Department of Energy Biomass Power program and the National Renewal Energy Laboratory's Directors Discretionary Fund. The Phillip Morris Corporation has supported part of this work and we thank Dr. Mohammad Hajaligol. Some of the electronic structure calculations were supported by a grant from the National Center for Supercomputer

Applications (NCSA Grant # CHE-980028n). Many aspects of this double-pulsed radical experiment and subsequent polarizations were discussed extensively with our friends Drs. Brad Rowland and Wayne Hess at the Pacific Northwest National Laboratory's EMSL Lab. We are indebted to Jim Kastengren and Donald David in the CIRES Instrument Design Facility for their advice and excellent workmanship. Paul Beckingham of the JILA Electronics Shop helped us design and build the electronics that drive the double pulse experiment.

Appendix A: Chemical Synthesis of $CD_3N{=}NCD_3$

The synthetic steps in this appendix are derived from a series of earlier publications.[15,16,18,43] We have made some small simplifications and we have found the steps below to be a convenient, reliable source of CD_3NNCD_3.

Step 1. d_6-Dimethyl Dibenzoylhydrazine.

$$C_6H_5CONHNHCOC_6H_5 + (CD_3O)_2SO_2 + NaOH \rightarrow C_6H_5CON(CD_3)N(CD_3)COC_6H_5$$

1,2-Dibenzoyl hydrazine (20 g, 83 mmol) was suspended in a sodium hydroxide solution (2%, 150 mL) with vigorous mechanical stirring. The temperature of the mixture was raised and maintained between 80 and 90 °C using a water bath before sodium hydroxide solution (50%, 63 mL) and d_6-dimethyl sulfate (Aldrich, 33 mL, 326 mMol) were added, dropwise and simultaneously from two pressure equalizing dropping funnels over 1 h. The mixture was stirred for a further 1 h at 80 °C and then placed in a refrigerator for 12 h, the resulting crystals were collected by filtration and washed with cold water (30 mL). The crude product was then crushed in chloroform (100 mL) and filtered. The chloroform filtrate was transferred to a separating funnel and washed successively with water (30 mL) and sodium chloride solution (saturated, 30 mL) before the solvent was removed in vacuo leaving a colorless oil that crystallized upon refrigeration. Recrystalization of the product (chloroform/ether/*n*-pentane) gave white crystals (8.4 g, 40%), which were collected by filtration.

Step 2. d_6-Dimethylhydrazine Hydrochloride.

$$C_6H_5CON(CD_3)N(CD_3)COC_6H_5 + HCl_{(conc)} \rightarrow (CD_3NHNH_2CD_3)^+Cl^-$$

d_6-Dimethyl dibenzoylhydrazine (8.4 g, 30 mmol) was dissolved in hydrochloric acid (37%, 34 mL) with stirring. The mixture was refluxed for 3 h, during which time benzoic acid crystallized. The reaction was cooled before a benzene/ether solvent mixture was added (1:1, 50 mL) and aqueous and organic phases were transferred to a separating funnel. The aqueous portion was extracted and washed a further three times with the organic solvent mixture (3×50 mL) before the water was removed by distillation and the crude product was dried under vacuum for 12 h. The resulting white solid (2.8 g, 96%) was used without further purification.

Step 3. d_6-Azobismethane.[15,18]

$$(CD_3NHNH_2CD_3)^+Cl^- + KOH \rightarrow CD_3NHNHCD_3 \quad \text{(i)}$$

$$CD_3NHNHCD_3 + HgO \rightarrow CD_3NNCD_3 \quad \text{(ii)}$$

d_6-Dimethylhydrazine hydrochloride (2.8 g, 28 mmol) was dissolved in the minimum amount of water (3 mL) with stirring and was neutralized by successive addition of potassium hydroxide pellets until pH = 7. The resulting solution was added dropwise over 0.5 h, under a stream of dry nitrogen, to a stirred suspension of mercuric oxide (10 g, 50 mmol) in water (5 mL). After passing through the reaction vessel, the nitrogen flow was directed through an efficient water-cooled condenser, followed by two glass traps connected to a gas manifold and cooled to −78 °C, and finally to a mineral oil bubbler. After complete addition of the d_6-dimethylhydrazine solution, the mixture was stirred for a further 0.5 h and then heated at 50 °C for 0.5 h and 60 °C for 0.2 h, after which time the glass traps were cooled in liquid nitrogen and isolated from the reaction vessel. The white solid visible in the traps was transferred by trap−trap distillation via a short drying tube (Drierite) to a test tube fitted with a Teflon tap. Upon removal from the coolant, the solid rapidly melted to give a colorless liquid (~0.5 mL, 30%, bp 1 °C), which could be reliably stored at −20 °C for several months.

Appendix B: Infrared Absorption Spectra of Methylperoxyl Isotopomers

Figure 7 is the matched set of depletion/266 nm polarization spectra for the $CH_3{}^{18}O{}^{18}O$ radical. We assign all the vibrational modes in the fingerprint region save for ν_{11} (this asymmetric CH_3 rock appears to be too weak for us to detect) and ν_{12} (beyond the range of our MCT detector). Notice that there are small, unassigned satellite bands associated with modes ν_5, ν_6, ν_7, and ν_8. These features appear in both the depletion and polarization spectra, and we are not completely certain of their identity; we tentatively ascribe them to methylperoxyl radicals occupying different matrix sites. Figure 8 is a comparison of the calculated UB3LYP harmonic modes (ω in red) with the experimental $CH_3{}^{18}O{}^{18}O$ modes (ν in black) in the fingerprint region. A number of impurities clutter the experimental spectrum: **E** is CH_3CH_3, **M** is CH_4, and **m** is CH_3OH. Figure 8 shows a reasonable fit of the $\{\omega\}$ in red to the corresponding $\{\nu\}$ features in black, but it is clear that the harmonic intensities $\{A\}$ are erratic. Depletion/polarization spectra for the CH stretching region are shown in Figure 9. We can clearly identify the a″ CH mode (ν_9), but only a single a′ mode is evident (ν_2). Figure 10 is a comparison of the UB3LYP harmonic CH modes in red with the experimental values in black. The complex, blended feature about 3030 cm^{-1} clearly contains both ν_1 and ν_9; Figure 9 permits a secure assignment of ν_9. The structured peaks at 2950 in both Figures 9 and 11 clearly contain ν_2; we have chosen the intense feature at 2953 cm^{-1} for ν_2.

Spectra for the $^{13}CH_3OO$ radical begin in Figure 11; this shows the depletion/266 nm polarization spectra for the ^{13}C isotopomer. The IR spectra for $^{13}CH_3OO$ are somewhat cluttered because we used $^{13}CH_3I$ as the $^{13}CH_3$ source. The decomposition of methyl iodide requires a significantly higher nozzle temperature and leads to more extensive radical fragmentation. All of this causes us more difficulties in the IR spectrum. Figure 12 is a comparison of the ab initio harmonic frequencies (red) to the experimental $^{13}CH_3OO$ bands (black). Figure 13 is a comparison of the CH harmonic frequencies to the experimental values. We were unable to measure a LD spectrum for $^{13}CH_3OO$ because our radical samples (resulting from $^{13}CH_3I$ decomposition) were so poor. The experimental bands in Figure 13 (ν_1, ν_9, and ν_2) are chosen by analogy with results for CH_3OO and $CH_3{}^{18}O{}^{18}O$.

Figure 14 shows the depletion/266 nm polarization spectra for the CD_3OO isotopomer fingerprint region; Figure 15 displays the comparison of the harmonic modes. Figure 16 is a view of the CD stretching region. We were unable to measure an LD spectrum for CD_3OO because our radical samples (resulting

from both CD_3NNCD_3 and CD_3I decomposition) were inadequate. As in the $^{13}CH_3OO$ isotopomer, the experimental CD_3OO bands in Figure 16 (ν_1, ν_9, and ν_2) are chosen by analogy with results for CH_3OO and $CH_3{}^{18}O{}^{18}O$.

References and Notes

(1) Ravishankara, A. R. *Annu. Rev. Phys. Chem.* **1988**, *39*, 367.

(2) Madronich, S.; Greenberg, J.; Paulson, S. Carbon-Containing Compounds. In *Atmospheric Chemistry and Global Change*, 1st ed.; Brasseur, G. P., Orlando, J. J., Tyndall, G. S., Eds.; Oxford University Press: New York, 1999; p 325.

(3) *Chemical Processes in Atmospheric Oxidation*; Le Bras, G., Ed.; Springer: Berlin, 1997; Vol. 3. Chapter 2, §2.1, 2.3, and 2.4.

(4) Finlayson-Pitts, B. J.; Pitts, J. N., Jr. *Science* **1997**, *276*, 1045.

(5) Lightfoot, P. D.; Cox, R. A.; Crowley, J. N.; Destriau, M.; Hayman, G. D.; Jenkin, M. E.; Moortgat, G. K.; Zabel, F. *Atmos. Environ.* **1992**, *26A*, 1805.

(6) Ellison, G. B.; Tuck, A. F.; Vaida, V. *J. Geophys. Res.-Atmos.* **1999**, *104*, 11633.

(7) Pruppacher, H. R.; Klett, J. D. *Microphysics of Clouds and Precipitation*, 2nd ed.; Kluwer Academic Publishing: Dordrecht, Holland, 1997; Chapter 9, Heterogeneous Nucleation. See §9.2, Ice Forming Nuclei, pp 309−360.

(8) Bertram, A. K.; Ivanov, A. V.; Hunter, M.; Molina, L. T.; Molina, M. J. *J. Phys. Chem. A.* **2001**, submitted.

(9) Tyndall, G. S.; Wallington, T. J.; Ball, J. C. *J. Phys. Chem.* **1998**, *102*, 2547.

(10) Friderichsen, A. V.; Radziszewski, J. G.; Nimlos, M. R.; Winter, P. R.; Dayton, D. C.; David, D. E.; Ellison, G. B. *J. Am. Chem. Soc.* **2001**, *123*, 1977.

(11) Nandi, S.; Arnold, P. A.; Carpenter, B. K.; Nimlos, M. R.; Dayton, D. C.; Ellison, G. B. *J. Phys. Chem. A* **2001**, *105*, 7514.

(12) Chen, P. *Spectroscopy and Photochemistry in Supersonic Jets*. Ph.D. Thesis, Chemistry, Yale, 1987.

(13) Kohn, D. W.; Clausberg, H.; Chen, P. *Rev. Sci. Instrum.* **1992**, *63*, 4003.

(14) Rohrs, H. W.; Wickham-Jones, C. T.; Ellison, G. B.; Berry, D.; Argrow, B. M. *Rev. Sci. Instrum.* **1995**, *66*, 2430.

(15) Renaud, R.; Leitch, L. C. *Can. J. Chem.* **1954**, *32*, 545.

(16) Morse, A. T.; Massiah, T. F.; Leitch, L. C. *Can. J. Chem.* **1959**, *37*, 1.

(17) Hatt, L. M. *J. Chem. Phys.* **1990**, *93*, 3161.

(18) Voss, M. *Adsorption and Reaction of Small Molecules and Radicals on Metal Alloys and Molecular Solids*. Ph.D. Thesis Thesis, Chemistry, University of Southern California, 1998.

(19) Brown, A. L.; Dayton, D. C.; Nimlos, M. R.; Daily, J. W. *Chemosphere* **2001**, *42*, 663.

(20) Clifford, E. P.; Wenthold, P. G.; Gareyev, R.; Lineberger, W. C.; DePuy, C. H.; Bierbaum, V. M.; Ellison, G. B. *J. Chem. Phys.* **1998**, *109*, 10293.

(21) Hunziker, J. E.; Wendt, H. R. *J. Chem. Phys.* **1976**, *64*, 3488.

(22) Pushkarsky, M. B.; Zalyubovsky, S. J.; Miller, T. A. *J. Chem. Phys.* **2000**, *112*, 10695.

(23) Goddard, W. A., III.; Harding, L. B. *Annu. Rev. Phys. Chem.* **1978**, *29*, 363.

(24) Bair, R. A.; Goddard, W. A., III. *J. Am. Chem. Soc.* **1982**, *104*, 2719.

(25) Blanksby, S. J.; Ramond, T. M.; Davico, G. E.; Nimlos, M. R.; Kato, S.; Bierbaumb, V. M.; Lineberger, W. C.; Ellison, G. B.; Okumura, M. *J. Am. Chem. Soc* **2001**, in press.

(26) Berkowitz, J.; Ellison, G. B.; Gutman, D. *J. Phys. Chem.* **1994**, *98*, 2744.

(27) Ochterski, J. W.; Petersson, G. A.; Montgomery, J. A. *J. Chem. Phys.* **1996**, *104*, 2598.

(28) Cotton, F. A. *Chemical Applications of Group Theory*, 3rd ed.; John Wiley & Sons: New York, 1990; Chapter 10.

(29) Pilar, F. L. *Elementary Quantum Chemistry*; McGraw-Hill: New York, 1968; see §14.7.

(30) Shimanouchi, T. *Tables of Molecular Vibrational Frequencies*; National Bureau of Standards, 1972; Vol. I.

(31) Frisch, M. J.; Trucks, G. W.; Schlegel, H. B.; Scuseria, G. E.; Robb, M. A.; Cheeseman, J. R.; Zakrzewski, V. G.; Montgomery, J. A., Jr.; Stratmann, R. E.; Burant, J. C.; Dapprich, S.; Millam, J. M.; Daniels, A. D.; Kudin, K. N.; Strain, M. C.; Farkas, O.; Tomasi, J.; Barone, V.; Cossi, M.; Cammi, R.; Mennucci, B.; Pomelli, C.; Adamo, C.; Clifford, S.; Ochterski, J.; Petersson, G. A.; Ayala, P. Y.; Cui, Q.; Morokuma, K.; Malick, D. K.; Rabuck, A. D.; Raghavachari, K.; Foresman, J. B.; Cioslowski, J.; Ortiz, J. V.; Baboul, A. G.; Stefanov, B. B.; Liu, G.; Liashenko, A.; Piskorz, P.; Komaromi, I.; Gomperts, R.; Martin, R. L.; Fox, D. J.; Keith, T.; Al-Laham, M. A.; Peng, C. Y.; Nanayakkara, A.; Gonzalez, C.; Challacombe, M.; Gill, P. M. W.; Johnson, B.; Chen, W.; Wong, M. W.; Andres, J. L.; Gonzalez, C.; Head-Gordon, M.; Replogle, E. S.; Pople, J. A., *Gaussian 98*, A.7; Gaussian Inc.: Pittsburgh, PA, 1998.

(32) Winter, P. *Photochemisty in the Condensed Phase: The Photodecompostion of CH_3CH_2COCl, and the production and detection of propargyl radical in an Argon matrix*. Ph.D. Thesis, Chemistry and Biochemistry, University of Colorado, 1999.

(33) Ase, P.; Bock, W.; Snelson, A. *J. Phys. Chem.* **1986**, *90*, 2099. Ase and co-workers studied the infrared absorption spectra of 10 isotopic variants of the methylperoxyl radical: CH_3OO, $CH_3{}^{16}O{}^{18}O$, $CH_3{}^{18}O{}^{16}O$, $CH_3{}^{18}O{}^{18}O$, $^{13}CH_3OO$, $^{13}CH_3{}^{18}O{}^{18}O$, CD_3OO, $CD_3{}^{16}O{}^{18}O$, $CD_3{}^{18}O{}^{16}O$, and $CD_3{}^{18}O{}^{18}O$.

(34) Cyvin, B. N.; Cyvin, S. J.; Snelson, A. *Z. Anorg. Allg. Chem.* **1986**, *542*, 193.

(35) Chettur, G.; Snelson, A. *J. Phys. Chem.* **1987**, *91*, 913.

(36) Chettur, G.; Snelson, A. *J. Phys. Chem.* **1987**, *91*, 3483.

(37) Chettur, G.; Snelson, A. *J. Phys. Chem.* **1987**, *91*, 5873.

(38) Michl, J.; Thulstrup, E. W. *Spectroscopy with Polarized Light*; VCH: New York, 1996.

(39) Wong, M. W. *Chem. Phys. Lett.* **1996**, *256*, 391.

(40) Scott, A. P.; Radom, L. *J. Phys. Chem.* **1996**, *100*, 16502.

(41) Jacox, M. E. *J. Mol. Spectrosc.* **1985**, *113*, 286.

(42) Jacox, M. E. *Chem. Phys.* **1994**, *189*, 149.

(43) Hatt, H. H. *Organic Syntheses*; Blatt, A. H., Ed.; 1943; Vol. II; p 208.

(44) Jacox, M. E. *Vibrational and Electronic Energy Levels of Polyatomic Transient Molecules*; American Chemical Society: Washington, DC, 1994.